Global and Planetary Change 257 (2026) 105267

Contents lists available at ScienceDirect

Global and Planetary Change

journal homepage: www.elsevier.com/locate/gloplacha

Tracing crustal thickness evolution of the Rodinia's peripheral orogens as recorded in the Yangtze Block, South China

Yiran Huang [a], Junyong Li [a,*], Xiaolei Wang [a], Zhidong Gu [b], Yue Guan [a]

[a] State Key Laboratory of Critical Earth Material Cycling and Mineral Deposits, Nanjing University, Nanjing 210023, China
[b] Research Institute of Petroleum Exploration and Development, PetroChina, Beijing 10083, China

ARTICLE INFO

Editor: Sun Jimin

Keywords:
Peripheral orogenesis
Rodinia
Yangtze Block
Crustal thickness
Detrital zircon

ABSTRACT

The Tonian (ca. 1000–720 Ma) magmatic belts along the western and northern margins of the Yangtze Block represent critical components of the long-lived peripheral orogenic system of the Rodinia supercontinent. Reconstructing their crustal thickness evolution is essential for understanding Neoproterozoic paleotectonics and paleoenvironments. In this study, we integrate Eu/Eu*-in-zircon crustal thickness proxy with U-Pb-Hf-O isotopes from Late Tonian and Cryogenian strata to revisit Rodinia's peripheral orogenesis as recorded in the Yangtze Block, South China. The results indicate the average orogenic crust may have thickened from ~40 to ~60 km during ca. 1000–920 Ma. Zircons of this age mainly present positive $\varepsilon_{Hf}(t)$ (+8.0 – +11.1) and mantle-like $\delta^{18}O$ (4.80–6.33 ‰) values. Combined with geologic observations, this thickening may result from both juvenile magmatic addition and crustal shortening. During ca. 850–750 Ma, a period of significant flare-ups of continental arc magmatism occurred, the crustal thickness fluctuated slightly and stabilized around 50 km. Zircons from this interval exhibit highly variable $\varepsilon_{Hf}(t)$ (−22.2 – +10.2) and $\delta^{18}O$ (1.6–10.6 ‰) values, reflecting active crustal recycling and mantle-crust differentiation. The maintenance of constant average crustal thickness during this interval is interpreted as reflecting spatial asynchrony and/or frequent temporal switching between advancing and retreating accretionary orogenies. Besides, our findings support that the Tonian peripheral orogen of Rodinia represent a transitional phase in the evolution of both crustal thickness and geothermal gradients, bridging the subduction orogenic styles of the Mesoproterozoic and Phanerozoic eras.

1. Introduction

The evolution of crustal thickness in orogens reflects the complex interplay between endogenous (such as magma accretion, lower crust recycling) and exogenous (such as erosion) processes over a long timescale (Larsen et al., 2014; Ducea et al., 2015; Farner and Lee, 2017). This dynamic evolution is intrinsically linked to the variation of paleotectonics and paleoenvironment and provides broader implications for ore formation and continental evolution (Lee et al., 2015; Lee and Tang, 2020; Cawood et al., 2022; Xiong et al., 2023a). Supercontinent's assembly and breakup coincide with continuous plate adjustments that trigger global-scale orogenies in its interior and exterior. Of them, the exterior orogenies involve long-lived oceanic subduction at the supercontinent's margins, giving rise to the peripheral orogenic system that displays histories of protracted magmatism, tectonism, metamorphism, weathering, and erosion (Murphy and Nance, 1991; Cawood et al., 2009, 2021). The peripheral orogenic system is hence supposed to fingerprint considerable crustal thickness variation over large spatial and temporal scales. However, how the crustal thickness evolved in the peripheral orogenic system of different supercontinents through Earth's history remains incompletely understood.

Rodinia and Pangea represent the most recent supercontinents in the geological record and show an evolutional coherency during their breakup, i.e., degree-2 mantle structure (two antipodal upwellings bisected by a meridional downwelling; Mitchell et al., 2021) with development of a near-continuous belt of subduction girdles at their exterior margins (Fig. 1A). One latest study on modern North America Cordillera orogen, which pertains to Pangea's peripheral orogenic system, has revealed it underwent two episodes of crust thickening since 200 Ma, with the thickest crust (~70 km) developing during the Middle-Late Cretaceous (Tang et al., 2024). However, research on the crustal thickness of the Rodinia's peripheral orogenic belt is limited. This raises

This article is part of a Special issue entitled: 'Interconnected orogenesis' published in Global and Planetary Change.

* Corresponding author.
E-mail address: ljy@nju.edu.cn (J. Li).

https://doi.org/10.1016/j.gloplacha.2025.105267
Received 29 April 2025; Received in revised form 9 September 2025; Accepted 20 December 2025
Available online 22 December 2025

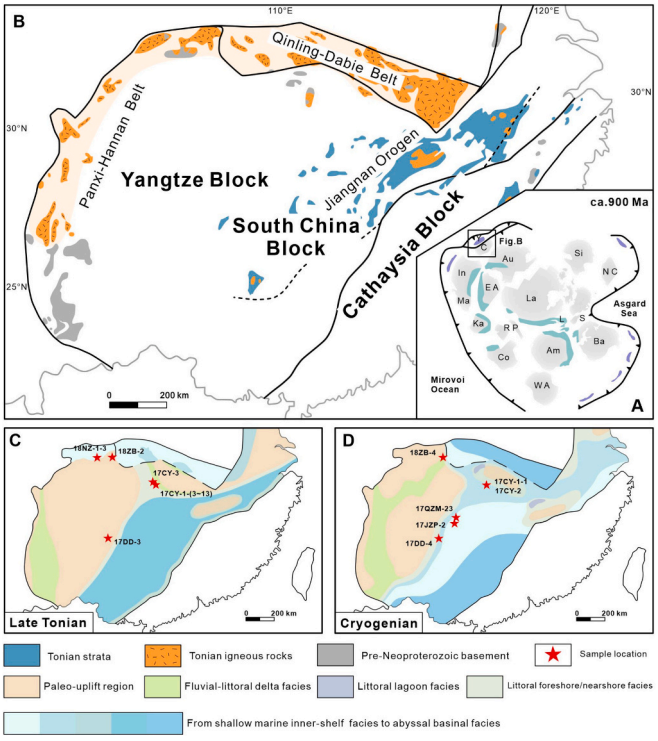

Fig. 1. Neoproterozoic geological background for the Yangtze Block, South China. (A) Schematic paleogeographic reconstruction of Rodinia at ca. 900 Ma showing Rodinia's peripheral orogenic system and the position of the Yangtze Block, adapted from Spencer et al. (2015), Cawood et al. (2018), and Yao et al. (2019). The early-stage (ca. 1.40–0.92 Ga) Rodinia's interior orogenic belts are marked in green, while the late-stage Rodinia's peripheral orogenic belts (ca. 1.03–0.53 Ga) are marked in purple. Au-Australia, Am-Amazonia, La-Laurentia, Si-Siberia, Ba-Baltica, Co-Congo, Ka-Kalahari, EA-East Antarctica, WA-West Africa, NC-North China, RP-Rio de Plate, Ma-Madagascar, In-India, Y-Yangtze, C-Cathaysia, L-Labador, S-Scotland. (B) Simplified geological map showing the distribution of the Tonian orogens (e.g., the Panxi-Hannan Belt and the Jiangnan Orogen) flanking the Yangtze Block, adapted from Zhao and Cawood (2012). (C&D) Paleogeographic maps (modified from Dong et al., 2024) of the Yangtze Block during the Late Tonian and Cryogenian (ca. 800–635 Ma) demonstrating that the western and northern regions of the block were predominantly paleo-uplift areas, whereas the southeastern part was primarily a sedimentation domain. The sample locations are marked on the maps. (For interpretation of the references to colour in this figure legend, the reader is referred to the web version of this article.)

questions regarding the crustal thickness evolution for Rodinia's peripheral orogens and whether it is comparable to their modern counterparts.

The Tonian (ca. 1000–720 Ma) magmatic belts on the western and northern margins of the Yangtze Block (South China), along with those in NW India, Seychelles, and Madagascar, have been proposed to be temporally and spatially linked (Wang et al., 2017b). They together constitute parts of Rodinia's peripheral orogenic system and serve as crucial research targets for deciphering the evolution of Neoproterozoic peripheral orogenic systems (Cawood et al., 2010, 2013b; Spencer et al., 2015; Wang et al., 2017a). In this study, we examine the crustal thickness evolution of Tonian orogens and associated tectono-magmatic processes in the Yangtze Block. Besides, we discuss variations of crustal thickness and geothermal state in the orogenic systems.

2. Geological background and samples

The Yangtze Block in the northwestern part of the South China Block is characterized by remarkable geological processes during the Neoproterozoic Era (Zhao and Cawood, 2012; Shu et al., 2021; Dong et al., 2024), which have resulted in widespread and well-exposed Neoproterozoic rock records across its territory. Overall, these geological processes exhibit a temporal transition from Tonian orogenesis to Cryogenian–Ediacaran sedimentation (Shu et al., 2021; Dong et al., 2024). The Tonian orogenesis is primarily manifested by two linearly-distributed orogens flanking the Yangtze Block, i.e., the Panxi-Hannan Belt to the west and northwest and the Jiangnan Orogen to the southeast (Fig. 1B; Wang et al., 2007; Zhao et al., 2021; Shu et al., 2021). The Panxi-Hannan Belt is characterized by voluminous Tonian arc-related felsic to intermediate plutons and minor mafic-ultramafic intrusions (Zhou et al., 2002; Zhao and Zhou, 2007, 2009; Dong et al., 2011, 2012), which is considered to have formed in response to a long-lived oceanic subduction event (lasting at least from ca. 970 to ca. 750 Ma; Li et al., 2024). However, the Jiangnan Orogen is mainly composed of Tonian sedimentary rocks and granites, and it is thought to have undergone accretionary orogenesis since ca. 970 Ma, culminating in the assembly of the Yangtze and Cathaysia blocks by ca. 820 Ma (Wang et al., 2014; Yao et al., 2019). During the Late Tonian, subduction orogeny might still be active in the Panxi-Hannan Belt, while extensional basins started to develop in the Jiangnan Orogen area. This kind of tectonic configuration resulted in a topographically high region in the west, characterized by weathering and erosion, and a topographically low region in the east, where shallow-marine to bathyal-abyssal clastic successions were deposited throughout the Cryogenian and Ediacaran (Cawood et al., 2012; Cawood et al., 2013a; Shu, 2012; Shu et al., 2021; Dong et al., 2024).

We investigated seven Late Tonian to Cryogenian stratigraphic sections from the northern, central, and southern domains of the Yangtze Block (hereafter designated NYB, CYB and SYB). Sample locations are marked on the paleogeographic map (Fig. 1C&D) and stratigraphic correlation diagram (Fig. 2). We conducted detrital zircon chronological and geochemical analyses for a total of nineteen sedimentary samples from these sections to reveal the properties and magmatic-tectonic processes of their provenance.

3. Analytical methods

Detrital zircon grains were separated by standard heavy and magnetic mineral separation techniques. The cathodoluminescence (CL) images were obtained using a cathode fluorescence probe mounted on a scanning electron microphotography. Based on these images, we selected more than 1000 spots on zircon grains for analyses of U–Pb–O–Hf isotopes and trace elements. All of the above analyses were conducted at the State Key Laboratory of Critical Earth Material Cycling and Mineral Deposits, Nanjing University.

3.1. Zircon U-Th-Pb isotopes

Zircon in situ U-Th-Pb isotopic and trace elemental analyses were performed on a Thermofisher Quad-ICP-MS mass spectrometer with a Resolution LR/S155 laser ablation system. The laser with a 193 nm wavelength was set to 29 μm in diameter, 5 Hz pulse rate, 80 mJ or 75 mJ energy. The integration duration for each zircon point was 96 s, including background for 20 s. The standard samples were determined every 8 or 10 data points, and the standard reference material was synthetic silicate glass (NIST SRM612; NIST SRM610) developed by the United States National Standards and Technology, inserted once for SRM612, twice for SRM610 before and after. The zircon 91,500 (1062 ± 4 Ma) and PLE (337.13 ± 0.37 Ma) as the external standard reference materials for age correction and instrument monitoring. The trace elements concentration calculations were corrected by the ^{29}Si internal standard method. The original data were pre-processed and adjusted by ICPMSDataCal (V9.5), and the age calculation and spectrum plotting were completed with Isoplot (ver. 3) and Excel. Ages older than 1500 Ma were utilized at ^{207}Pb/^{206}Pb, and those younger than 1500 Ma were utilized at ^{206}Pb/^{238}U (Spencer et al., 2016). The ages and trace element

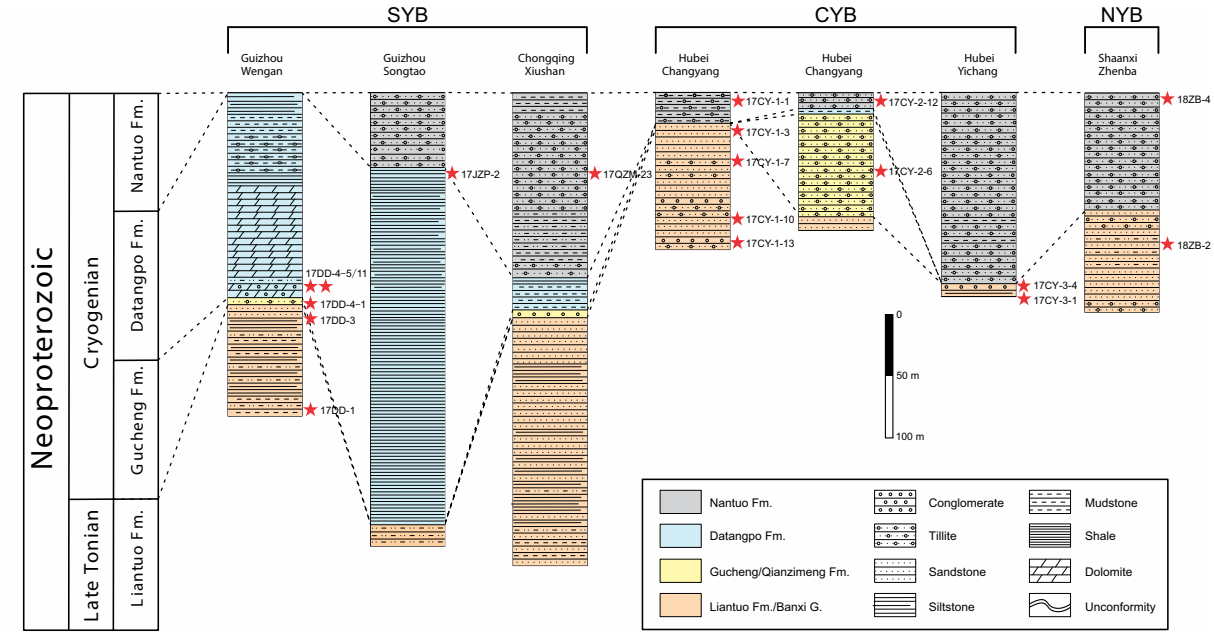

Fig. 2. The stratigraphic columns of the studied Late Tonian to Cryogenian sedimentary sections with sample locations marked. These samples are classified into three groups according to their geographic locations within the Yangtze Block: northern (NYB), central (CYB), and southern (SYB) regions.

contents of analyzed zircon grains were reported in Supplementary Dataset 1.

3.2. Zircon O isotope

Zircon oxygen isotopic analysis was performed using a Cameca IMS-1300HR[3] secondary-ion mass spectrometry (SIMS). The ion source was a cesium source ($^{133}Cs^{+}$), the $^{133}Cs^{+}$ primary ion beam was accelerated at 10 kV with an intensity of ~2 nA, focused to a region of ϕ 10 μm on the sample surface, and the analysis spot diameter was about 20 μm (beam diameter was 10 μm and grating was 10 μm). Oxygen isotopes were measured in multi-collector mode using two off-axis Faraday cups. Instrumental mass fractionation (IMF) correction was performed on the measured oxygen isotope data using the Penglai zircon standard ($\delta^{18}O_{SMOW} = 5.31 \pm 0.5$ ‰; Li et al., 2010), which was analyzed once every four unknowns. And using a sample-standard bracketing method with Qinghu as the external zircon standard sample, which was analyzed once every eight unknowns (Li et al., 2021a).

3.3. LA-MC-ICP-MS zircon Lu—Hf isotope

Zircon Lu—Hf isotopic analyses were obtained using a GeoLas 193 nm laser-ablation system attached to a Neptune (Plus) MC-ICP-MS. The spots for Hf isotope analyses were placed at the same spot as the previous laser U—Pb dating with a diameter of 44 μm. Masses ^{172}Yb, ^{173}Yb, ^{175}Lu, $^{176}Hf + Yb + Lu$, ^{177}Hf, ^{178}Hf, ^{179}Hf, and ^{180}Hf were measured in Faraday cups. Hf reference solution JMC475 was analyzed during an analytical session to allow normalization of fundamental mass spectrometer performance. Measuring ^{172}Yb and ^{175}Lu to correct for the interference of ^{176}Yb and ^{176}Lu to ^{176}Hf. Reference zircon Mudtank and 91,500 were used to monitor the accuracy and precision of Hf isotope ratios and instrumental drift with respect to the Lu/Hf ratios. εHf values were calculated relative to the chondritic values of Bouvier et al. (2008) ($^{176}Lu/^{177}Hf = 0.0336$; $^{176}Hf/^{177}Hf = 0.282785$).

4. Results

4.1. Provenance characteristics

We obtained 1328 effective age data of detrital zircon after eliminating discordant ages. Age distributions show three prominent clusters: 1000–720 Ma (75 %; $n = 994$), ca. 2000 Ma (11 %; $n = 153$), and ca. 2500 Ma (4 %; $n = 52$). Samples from NYB, CYB, and SYB have Tonian (1000–720 Ma) detrital zircons of 96 %, 61 %, and 86 % respectively, and their zircon age spectra consistently display peaks between 810 and 770 Ma (Fig. 3). Therefore, these Late Tonian to Cryogenian sedimentary domains are dominated by Tonian provenances. According to paleogeography (Fig. 1C&D), the majority of Tonian detrital zircon should be sourced from the Tonian (1000–720 Ma) magmatic belts (paleo-uplifts) in the northern and/or western areas of the Yangtze Block. On the other hand, all the Tonian detrital zircons in this study display (1) geochemical signatures ranging from I-type to hybrid S-type (Fig. 4A) and (2) continental arc geochemical characteristics (Fig. 4B). Additionally, numerous Archean-Paleoproterozoic detrital zircons found in CYB samples (Fig. 3B) were most likely sourced from nearby metamorphic-plutonic complexes (e.g., the Kongling Complex) in the Yangtze Block's interior (e.g., Gao et al., 2011; Chen et al., 2020).

Hf—O isotopes in Tonian detrital zircons could further delineate magmatic processes in the provenances (Fig. 5). Zircon Hf isotopes can reveal whether the host magmas originated from a juvenile source, enriched continental source, or a mixture of both (Kemp et al., 2007), while zircon O isotopes can record whether involving supracrustal or hydrothermally altered materials during the formation of the host magmatic rocks (Valley et al., 2003). For the NYB samples, the Tonian zircons mainly present $\varepsilon_{Hf}(t)$ values clustering above the CHUR line (up to +10.4) (Fig. 5). Their $\delta^{18}O$ values evolve from mantle-like to elevated levels from 1000 to 850 Ma, followed by more variable values (1.57–10.60 ‰) during 850–720 Ma (Fig. 5). For the CYB samples, zircons display depleted Hf [$\varepsilon_{Hf}(t)$ mainly from +8.0 to +14.7] and mantle-like O isotopic compositions (4.80–6.47 ‰) during 1000–850 Ma, followed by more variable Hf—O isotopic compositions during 850–720 Ma (Fig. 5). For the SYB samples, the Tonian zircons cluster within the 850–720 Ma age range and display a wide range of both $\varepsilon_{Hf}(t)$ and $\delta^{18}O$ values (Fig. 5). Overall, Tonian zircons from samples of three regions

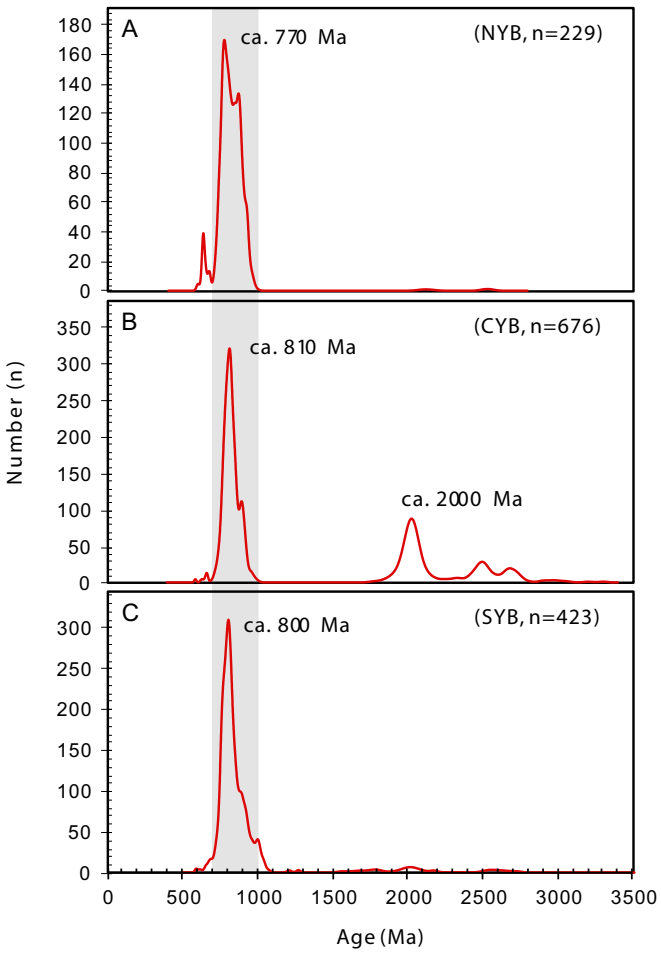

Fig. 3. The detrital zircon age spectrum diagram for Neoproterozoic strata from three domains of the Yangtze Block (NYB, CYB, and SYB).

depict similar magmatic and crustal evolutional histories in their provenance (i.e., Tonian orogens). The orogens were dominated by juvenile magmatism and crustal growth prior to ca. 850 Ma. Following were more complex magmatic processes relating to mantle-crust differentiation during ca. 850–720 Ma, involving coupled juvenile crustal growth and reworking of juvenile and ancient crust.

4.2. Crustal thickness estimation

Recent studies have demonstrated that the zircon europium anomaly (chondrite-normalized Eu/Eu*, Eu* = $\sqrt{Sm^{*}Gd}$) can serve as a reliable proxy for tracing crustal thickness evolution in magmatic arcs and orogens (Tang et al., 2021, 2024). The method is based on the principle that zircons crystallizing from high-pressure-differentiated melts (I- or A-type) tend to have elevated Eu/Eu* values, primarily due to the suppression of plagioclase crystallization and the endogenic oxidation of Eu^{2+} resulting from garnet fractionation (the garnet prefers to sequester Fe^{2+} over Fe^{3+} from the melt, and its fractionation will increase $Fe^{3+}/\sum Fe$ and thereby the oxygen fugacity of the residual melt; Tang et al., 2018, 2021). Therefore, when magmatic differentiation occurs beneath the base of the crust, the Eu/Eu* of zircon is expected to show a positive correlation with crust thickness (Tang et al., 2021). The zircon Eu/Eu* crustal thickness proxy has been widely applied to various orogenic belts, e.g., Himalayan and Cordilleran orogens (Tang et al., 2021, 2024; Wu et al., 2023a), and its reliability has been further supported by other crust thickness indicators (e.g., whole rock La/Yb) and by geological observations (Tang et al., 2021, 2024). In addition, it is noteworthy that a sufficiently large dataset is required when applying the zircon Eu/Eu* proxy in order to mitigate the influence of local magmatic processes (e.g., crustal assimilation) on the overall results (Tang et al., 2024).

We reconstruct the crustal thickness evolution of the Tonian orogens in the Yangtze Block in a similar method (Fig. 5&6C). We refine the dataset on the basis of trace elemental filtering criteria described in Tang et al. (2024) and acquire 391 effective geochemical data of Tonian zircon after removing ~24 % of the original data. The result shows that the estimated crustal thickness for Tonian orogens is generally higher than 40 km (Fig. 5). Samples from the three different regions document slightly different tendencies in crustal thickness evolution: (1) both the NYB and SYB samples record one remarkable crustal thickening during 950–920 Ma and once slight crustal thickening during 820–760 Ma; (2) the CYB samples record that the crustal thickness slightly decreases from about 60 to 50 km during 980–920 Ma and stabilized at ~50 km thereafter. However, their Tonian provenances record similar magmatic and crustal evolutionary histories from perspectives of zircon Hf—O isotopic (see $\varepsilon_{Hf}(t)$ and $\delta^{18}O$ in Fig. 5) and Eu/Eu* proxies. This enables us to integrate all analyzed regional geochemical data to depict crust-thickness evolution of the peripheral orogens of the Rodinia as recorded in the Yangtze Block (Fig. 6).

The LOESS (Locally Estimated Scatterplot Smoothing) curve in Fig. 6C defines three evolutionary stages for crustal thickness: (1)

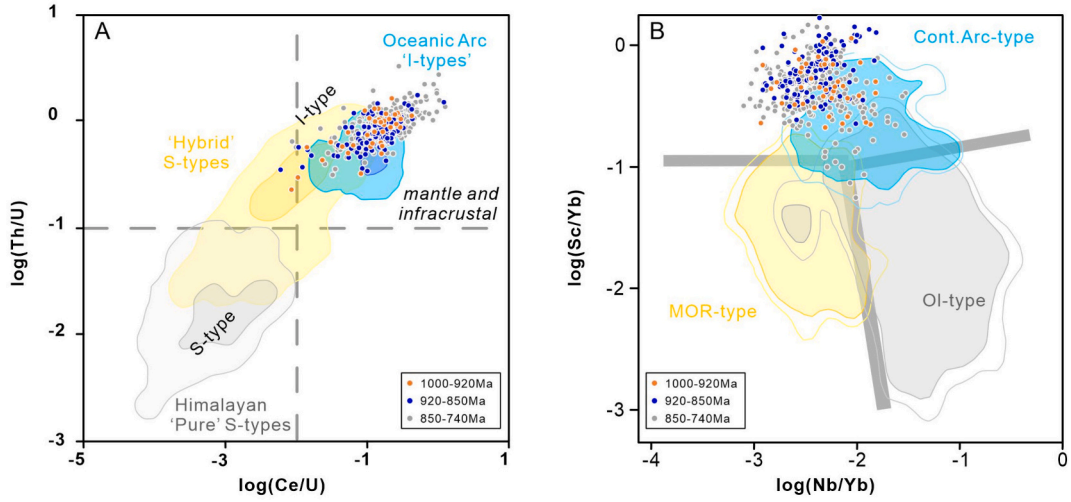

Fig. 4. The trace element distributions of the Tonian detrital zircons resemble those of I- to hybrid S-types and continental arc igneous rocks. (A) Th/U vs. Ce/U logarithmic diagram (Roberts et al., 2024). (B) Sc/Yb vs. Nb/Yb logarithmic diagram (Grimes et al., 2015).

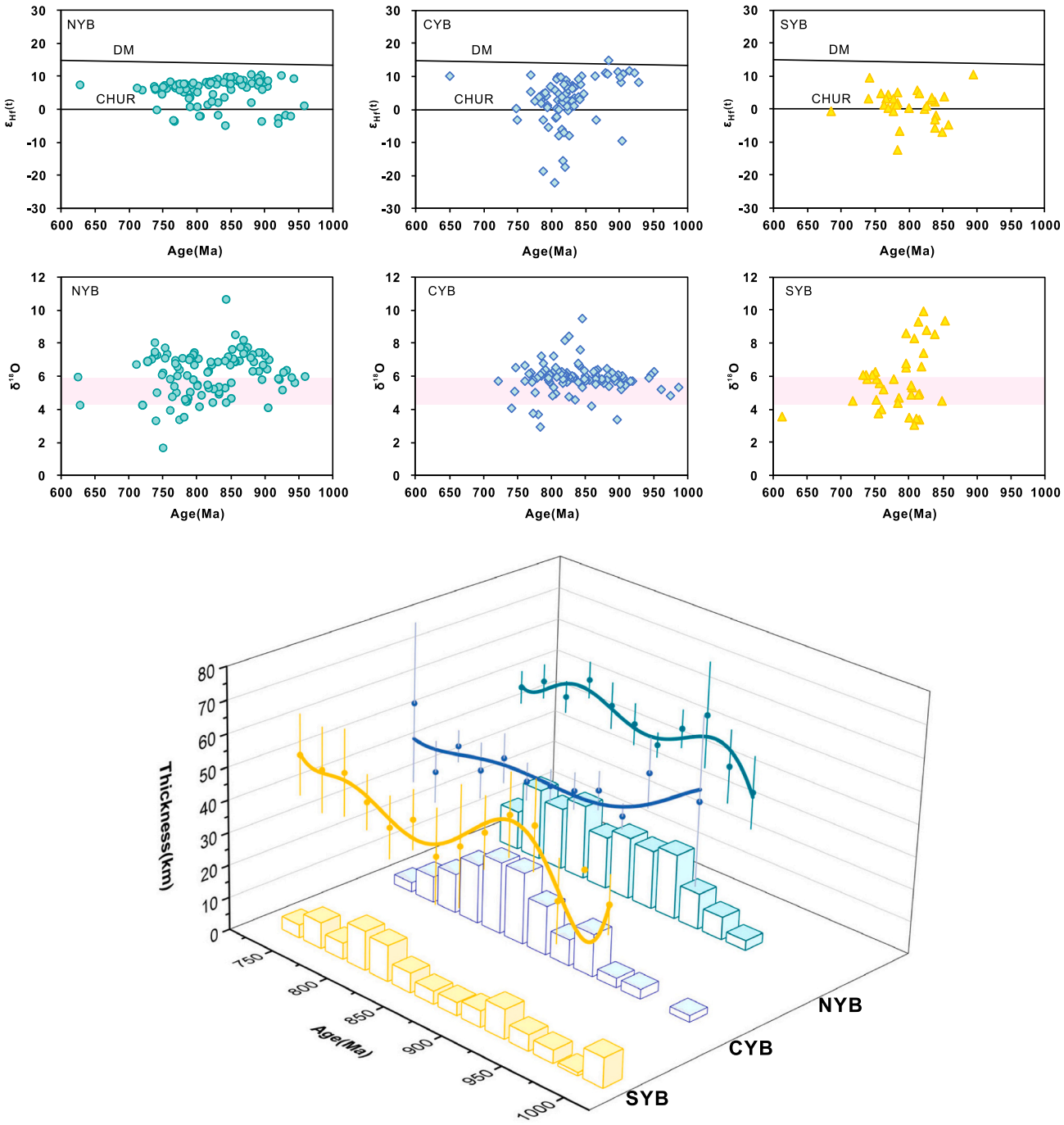

Fig. 5. Temporal variation in zircon Hf—O isotopes and crustal thickness from three domains of the Yangtze Block (NYB, CYB, and SYB). The pink light band denotes the mantle O isotopic range (5.3 ± 0.6 ‰, Valley et al., 1998). The CHUR represents the chondritic uniform reservoir evolution line, and DM represents the depleted mantle evolution line, defined by present-day $^{176}Hf/^{177}Hf = 0.28325$ and $^{176}Lu/^{177}Hf = 0.0384$ (Griffin et al., 2000, 2004). The crustal average thickness was calculated using the formula of Tang et al. (2021) with a 20 Myr sliding window and step size. The curves are fitted using polynomial regression, and the bar chart shows the number of detrital zircon samples within each window. (For interpretation of the references to colour in this figure legend, the reader is referred to the web version of this article.)

thickening from about 40 to 60 km during 1000–920 Ma; (2) thinning to 50 km during 920–850 Ma; (3) stabilization at 50–55 km during 850–750 Ma. The thickness data are shown as 10-Myrs binned averages with error bars indicating ±2SEM (calculated by error propagation). The LOESS curve and enveloped confidence intervals are generated in MATLAB software using 1000 bootstrap iterations and a span parameter of 0.5. Furthermore, we employed an independent proxy (i.e., whole-rock La/Yb-based crustal thickness proxy; Profeta et al., 2015) to validate the results derived from the Eu/Eu* proxy. We compiled published whole-rock La/Yb data from Tonian igneous rocks along the northwestern margin of the Yangtze (Supplementary Dataset 2) and applied a filter to select low-magnesium, intermediate calc-alkaline rocks

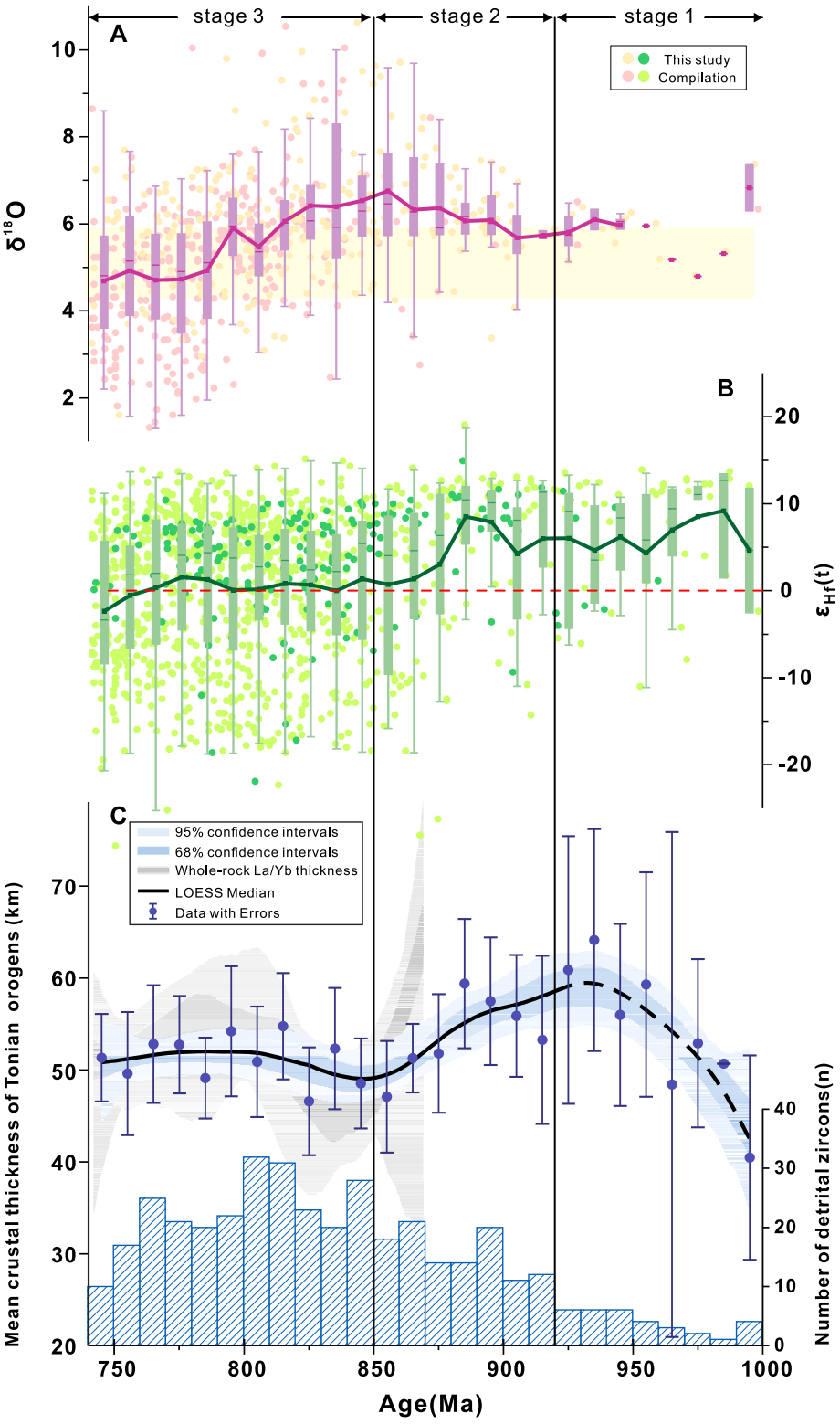

Fig. 6. Temporal evolution of zircon Hf—O isotopic compositions and mean zircon-Eu/Eu*-based crustal thickness for Tonian peripheral orogens of Rodinia as recorded in the Yangtze Block. Some zircon Hf—O data are compiled from Sun et al. (2009), Zhu et al. (2009), Wang et al. (2011, 2012, 2013), Yang et al. (2016, 2018), Liu et al. (2018), Li et al. (2020), Huang et al. (2021a, 2021b), Zhao et al. (2022). In Fig. 6A&B, the data are binned in 10 Myr intervals, with box boundaries representing the upper and lower quartiles, whiskers extending to the maximum and minimum values, and discrete points denoting outliers. In Fig. 6C, a sliding window with a 10 Myr step size is applied, and error bars correspond to ±2 standard errors. The black curve was obtained using LOESS smoothing with 1000 bootstrap resampling, where solid segments indicate bins containing ≥10 samples and dashed segments represent those containing <10 samples. The blue and grey envelopes represent the 68 % and 95 % confidence intervals from the zircon Eu/Eu* and whole-rock La/Yb proxies, respectively. The detailed calculation results are presented in Supplementary Dataset 2. (For interpretation of the references to colour in this figure legend, the reader is referred to the web version of this article.)

containing 55–68 wt% SiO_2 (Profeta et al., 2015). Data for the 1000–870 Ma intervals are lacking due to scarcity of igneous rock records from this period, consistent with the low abundance of 1000–870 Ma zircons in the detrital zircon age histogram (Fig. 6C). The whole-rock La/Yb-derived crustal thickness estimates are displayed as a grey envelope in Fig. 6C, which encompasses the zircon Eu/Eu* results in 870–750 Ma interval. Moreover, before 850 Ma, the crustal thickness shows a decreasing trend, consistent with the zircon Eu/Eu*-thickness estimates. We think the zircon Eu/Eu* proxy is robust and can be cross-validated with the independent whole-rock La/Yb proxy.

5. Discussion

5.1. Temporal evolution of crustal thickness in Tonian orogens

Integrated Hf—O isotopes and Eu/Eu* proxies from detrital zircons can provide insights into coupled crustal thickness evolution and related tectonic-magmatic processes for the source orogens (Tang et al., 2021). In this study, three different Late Tonian to Cryogenian sedimentary domains in the Yangtze Block (NYB, CYB, and SYB) consistently exhibit a major provenance of the Tonian orogens to the north and/or west of the block, which have been interpreted to be formed through accretionary orogenesis at the periphery of the Rodinia supercontinent (Li et al., 2024; Wu et al., 2024).

The covariation between Hf—O isotope and crustal thickness, combined with observed geological evidence, is an indispensable part of our interpretation of the temporal evolution of crustal thickness. We will discuss each of the three stages mentioned above in turn. During 1000–920 Ma, the crustal thickness increased rapidly from ~40 to ~60 km (Fig. 6C). This thickening event is supported by both zircon isotopic and geologic evidence. First, zircon Hf—O isotopes reveal a significant mantle contribution to magmatism during this period (Fig. 6A&B). Second, several magmatic records of this age have been identified along the western and northern margins of the Yangtze Block and are interpreted to have formed in an island-arc setting. These include ca. 970 Ma Tongmuliang volcanic rocks, ca. 985–950 Ma Changba, and ca. 950–936 Ma Sanchazi igneous rocks (Li et al., 2018; Wu et al., 2019; Wu et al., 2023a, 2023b). Third, the terranes accretion (Li et al., 2021a) and compressive tectonism and metamorphism may have occurred during this stage (our unpublished data). Taken together, three lines of evidence suggest that the rapid crustal thickening was driven by a combination of juvenile magmatic addition and crustal shortening.

Between 920 and 850 Ma, the crustal thickness underwent a ~ 10 km reduction over 60 Myr and finally reached ~50 km by ca. 850 Ma (Fig. 6C). This crustal thinning is somewhat puzzling considering the lack of magmatic records and extensional geologic evidence. We attribute this thinning to arc-root foundering, consistent with subduction orogenic cyclicity (DeCelles et al., 2009). The zircon $\varepsilon_{Hf}(t)$ values exhibit a decreasing trend but remain overall positive (+2.0 − +14.7), indicating enhanced crust-mantle interaction without triggering large-scale remelting of ancient crust. We propose that delamination of the arc root may have induced partial melting of juvenile crustal materials. Furthermore, the delamination could have created sufficient accommodation space beneath the arc crust, paving the way for subsequent large-volume magma recharge (Dickinson, 2004; DeCelles et al., 2009; Spencer et al., 2019). This process may have contributed to the pronounced magmatic flare-ups observed in the Yangtze Block between 850 and 750 Ma.

During ca. 850–750 Ma, zircons present a wide range of $\varepsilon_{Hf}(t)$ (−22.2 − +10.2) and $\delta^{18}O$ (1.57–10.60 ‰) values, with average $\varepsilon_{Hf}(t)$ values close to zero and a progressive decrease in average $\delta^{18}O$ from 6.54 ‰ to 4.36 ‰ (Fig. 6A&B). These variations suggest various types of magmatism associated with both juvenile crustal growth and the reworking of juvenile and ancient crustal components. Throughout this interval, the average orogenic crust thickness remained relatively stable at ~50 km (Fig. 6C). Considering the active tectonism and widespread magmatism within the Yangtze Block during this period (Zhao et al., 2021; Dong et al., 2024; Wu et al., 2024). We interpret the sustained stability of the average crustal thickness not as a static or stagnant state of the crust, but rather as a dynamic balance achieved through internal adjustments. This dynamic balance suggests that crustal thickening (via magmatic addition and crustal shortening) was effectively offset by crustal thinning (via arc-root foundering and lithospheric extension) within successful 10-Myr intervals during ongoing orogenesis (Fig. 6C). Such a balance is consistent with previously proposed tectonic models, including: (1) the coexistence of retreating and advancing accretionary orogenies in different segments of the continental margin (Zhao et al., 2019); and (2) the frequent alternations between retreating and advancing accretionary orogenies, with switching intervals of less than 30 Myr, as suggested by Wu et al. (2023a, 2023b). The spatial asynchrony and/or frequent temporal switching between retreating and advancing accretionary orogenies is supported by geological observations, as reflected in the widespread coexistence of arc-related igneous rocks (Zhu et al., 2019; Zhao et al., 2019, 2021), regional metamorphic rocks (Wang et al., 2020; Li et al., 2021a; Li et al., 2024), as well as extension-related A-type granites (Huang et al., 2008; Zhao et al., 2008), mafic dyke swarms (Zhang et al., 2009; Xiong et al., 2023b), and volcanic-sedimentary basins (Gu and Wang, 2014) within the orogenic belt.

5.2. Implications for Rodinia's Peripheral Orogenesis

Rodinia is a major Proterozoic supercontinent in Earth's history. Its assembly and subsequent breakup corresponded to secular changes in orogenic styles: i.e., early-stage (ca. 1.40–0.92 Ga) collisional orogenesis within Rodinia's interior to late-stage (ca. 1.03–0.53 Ga) accretionary orogenesis along its periphery (Cawood et al., 2016). The Rodinia's interior collisional orogens mainly developed on Laurentia, Amazonia and Batica (Johansson, 2009; Hynes and Rivers, 2010; Cawood and Pisarevsky, 2017). These mid-Proterozoic collisional orogens exhibit hotter and thinner crust with weaker crustal rheology (the elevated temperature weakens the rheology of the crust, diminishing its capacity to sustain topography) relative to their modern counterparts. This has been interpreted as a result of prolonged mantle heat influx and multi-episode crustal thinning events prior to Rodinia's assembly-related collisional orogeny (Spencer et al., 2021; Brudner et al., 2022). For example, a case study of the Grenville collisional orogen (ca. 1.25–0.98 Ga) estimates a maximum crustal thickness of ~60 km, which is up to 20 km thinner than that of the modern Himalayan-Tibetan orogen (Brudner et al., 2022).

This study offers a snapshot of the evolution of Rodinia's peripheral orogens as recorded in the Tonian Yangtze Block. First, crustal thickness estimates remained within the range of 50–60 km over a prolonged timescale (> 100 Myr), exceeding the global mean thickness of active continental crust at the same period (~40–45 km; Tang et al., 2021; Fig. 7). This may suggest that Rodinia's periphery developed a thicker orogenic crust than its interior. Second, Tonian crustal thicknesses are systematically higher than those of the Mesoproterozoic (~40–45 km), yet remain lower than modern counterparts such as the Cordilleran orogens, an Andes-type orogen where crustal thickness can exceed 70 km during thickening periods (Tang et al., 2024) (Fig. 7). Third, the Tonian orogens in the Yangtze Block exhibit relatively minor fluctuations in crustal thickness (Fig. 6C), in contrast to the episodic thickening in Cordilleran orogen (Tang et al., 2024).

Crustal thickness is closely linked to crustal rheology, which is controlled by the geothermal state and consequently, by metamorphic gradients (Brown and Johnson, 2019; Spencer et al., 2021). Elevated metamorphic thermobaric ratios (T/P) are commonly associated with mechanically weak crust and limited topographic elevation, as exemplified by Mesoproterozoic orogens characterized by hot, thin, and low-standing crust (Chardon et al., 2009; Gerya, 2014; Perchuk et al., 2018; Spencer et al., 2021). In contrast, Phanerozoic orogens generally exhibit

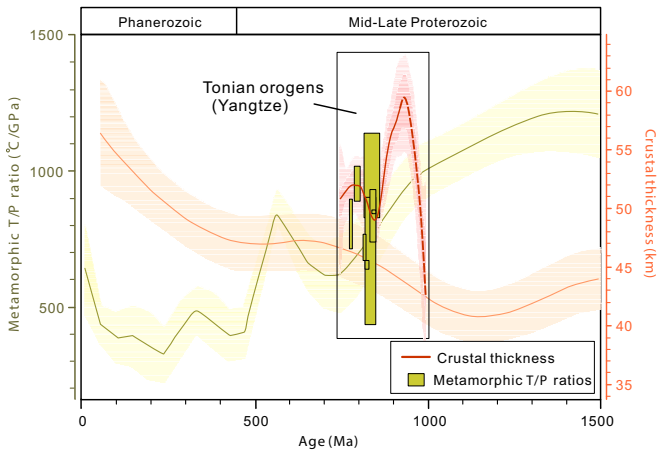

Fig. 7. Diagram showing the secular evolution of crustal thickness and geothermal regimes from the Mesoproterozoic to the Phanerozoic orogens along active continental margins, modified after Cawood (2020) and Roberts et al. (2022). The orange uncertainty band and curve are an estimate of the global mean thickness of active continental crust using the zircon Eu/Eu* proxy (Tang et al., 2021). The yellow band and curve are a smoothing trend of metamorphic thermobaric ratios through the global metamorphic record (Brown and Johnson, 2019). The solid and dashed curves with red indicate the estimated variations of crustal thickness for Rodinia's peripheral orogens as recorded in the Yangtze Block. The brown solid boxes represent the compiled Tonian metamorphic thermobaric ratios recorded in the Yangtze Block (Wang et al., 2020; Li et al., 2021a, 2021b, 2022, 2024; He et al., 2023; Yang et al., 2024; Guo et al., 2024). (For interpretation of the references to colour in this figure legend, the reader is referred to the web version of this article.)

lower metamorphic thermobaric ratios and higher topographic elevation, accompanied by development of *HP-LT* (blueschist) and ultrahigh-*P* metamorphic assemblages (Brown and Johnson, 2019; Roberts et al., 2022). The Neoproterozoic is widely interpreted as a transitional period in subduction style, shifting from 'hot and shallow' to 'cold and steep' (Hawkesworth et al., 2016; Palin et al., 2020). Within this framework, Tonian metamorphic records (880–750 Ma) from the Yangtze Block exhibit intermediate thermobaric ratios, falling between typical Mesoproterozoic and Phanerozoic values (Fig. 7), and thus may reflect an intermediate rheological state of the orogenic crust. This transitional geothermal regime may account for: (1) the absence of blueschist and ultrahigh-pressure metamorphic assemblages, which are diagnostic of cold Phanerozoic subduction zones (Stern, 2005; Brown, 2014); (2) the scarcity of anorthosite-mangerite-charnockite-granite suites, which are characteristic of Mesoproterozoic magmatic provinces and are formed through prolonged magma differentiation and sustained heat/magma supply (Ashwal and Bybee, 2017). Therefore, the Rodinia's peripheral orogens during the Tonian period could serve as a transitional phase in the evolution of both crustal thickness and geothermal gradients, bridging the subduction orogenic styles of the Mesoproterozoic and Phanerozoic eras (Fig. 7). These transitional features are likely also reflected in broader magmatic and crustal evolutional processes, shaping the distinctive geodynamic character of Tonian orogenesis along Rodinia's margins.

6. Conclusions

Detrital zircons from the Tonian orogenic belt reveal that the average crustal thickness primarily ranges between 50 and 60 km throughout the whole Tonian period, which supports a protracted subduction orogeny and arc-related magmatism along the northwestern margin of the Yangtze Block. Combined with geologic observations and zircon Hf—O isotopes, we suggest that the early-stage (1000–920 Ma) crustal thickening is driven by both magmatic addition and juvenile accretion. The subsequent crustal thinning during 920–850 Ma is interpreted as a result of the foundering of the arc-root. The late-stage (850–750 Ma) stable crustal thickness may reflect spatial asynchrony and/or frequent temporal switching between the two types of accretionary orogenies (retreating and advancing). Moreover, both the crustal thickness and metamorphic *T/P* ratios of Tonian orogens in the Yangtze Block reflect a secular transition in the geodynamic regime and crustal rheology from the Mesoproterozoic to the Phanerozoic. These transitional characteristics may also be reflected in the broader magmatic and crustal evolutionary processes in the Neoproterozoic.

CRediT authorship contribution statement

Yiran Huang: Writing – original draft, Investigation, Formal analysis, Data curation. **Junyong Li:** Writing – review & editing, Visualization, Supervision, Resources, Project administration, Methodology, Investigation, Funding acquisition, Conceptualization. **Xiaolei Wang:** Validation, Supervision, Conceptualization. **Zhidong Gu:** Resources, Project administration. **Yue Guan:** Methodology.

Declaration of competing interest

The authors declare that they have no known competing financial interests or personal relationships that could have appeared to influence the work reported in this paper.

Acknowledgement

This work was financially supported by the National Natural Science Foundation of China (Nos. 42202053 and 42025202), and the open research fund (2025-Z01) of the State Key Laboratory of Critical Earth Material Cycling and Mineral Deposits, Nanjing University. We thank H. Hu for assistance with LA-ICP-MS analyses, J.N. Chen for zircon Hf isotope analyses. We thank two anonymous reviewers for their detailed and constructive comments that improved the paper.

Appendix A. Supplementary data

Supplementary data to this article can be found online at https://doi.org/10.1016/j.gloplacha.2025.105267.

Data availability

The Supplementary Dataset 1 for detrital zircon U-Pb-Hf-O and trace elemental data and Supplementary Dataset 2 for crustal thickness estimation are available at https://doi.org/10.6084/m9.figshare.28890248.

References

Ashwal, L.D., Bybee, G.M., 2017. Crustal evolution and the temporality of anorthosites. Earth Sci. Rev. 173, 307–330. https://doi.org/10.1016/j.earscirev.2017.09.002.
Bouvier, A., Vervoort, J.D., Patchett, P.J., 2008. The Lu-Hf and Sm-Nd isotopic composition of CHUR: constraints from unequilibrated chondrites and implications for the bulk composition of terrestrial planets. Earth Planet. Sci. Lett. 273 (1–2), 48–57. https://doi.org/10.1016/j.epsl.2008.06.010.
Brown, M., 2014. The contribution of metamorphic petrology to understanding lithosphere evolution and geodynamics. Geosci. Front. 5 (4), 553–569. https://doi.org/10.1016/j.gsf.2014.02.005.
Brown, M., Johnson, T., 2019. Time's arrow, time's cycle: Granulite metamorphism and geodynamics. Mineral. Mag. 83 (3), 323–338. https://doi.org/10.1180/mgm.2019.19.
Brudner, A., Jiang, H.H., Chu, X., Tang, M., 2022. Crustal thickness of the Grenville orogen: a Mesoproterozoic Tibet? Geology 50 (4), 402–406. https://doi.org/10.1130/G49591.1.
Cawood, P.A., 2020. Earth matters: a tempo to our planet's evolution. Geology 48, 525–526. https://doi.org/10.1130/focus052020.1.
Cawood, P.A., Pisarevsky, S.A., 2017. Laurentia-Baltica-Amazonia relations during Rodinia assembly. Precambrian Res. 292, 386–397. https://doi.org/10.1016/j.precamres.2017.01.031.

Cawood, P.A., Kröner, A., Collins, W.J., Kusky, T.M., Mooney, W.D., Windley, B.F., 2009. Accretionary orogens through Earth history. Geol. Soc. London. https://doi.org/10.1144/SP318.1, p. 0.
Cawood, P.A., Strachan, R., Cutts, K., Kinny, P.D., Hand, M., Pisarevsky, S., 2010. Neoproterozoic orogeny along the margin of Rodinia: Valhalla orogen, North Atlantic. Geology 38 (2), 99–102. https://doi.org/10.1130/G30450.1.
Cawood, P.A., Hawkesworth, C.J., Dhuime, B., 2012. Detrital zircon record and tectonic setting. Geology 40 (10), 875–878. https://doi.org/10.1130/G32945.1.
Cawood, P.A., Hawkesworth, C.J., Dhuime, B., 2013a. The continental record and the generation of continental crust. Geol. Soc. Am. Bull. 125, 14–32. https://doi.org/10.1130/B30722.1.
Cawood, P.A., Wang, Y.J., Xu, Y.J., Zhao, G.C., 2013b. Locating South China in Rodinia and Gondwana: a fragment of greater India lithosphere? Geology 41 (8), 903–906. https://doi.org/10.1130/G34395.1.
Cawood, P.A., Strachan, R.A., Pisarevsky, S.A., Gladkochub, D.P., Murphy, J.B., 2016. Linking collisional and accretionary orogens during Rodinia assembly and breakup: Implications for models of supercontinent cycles. Earth Planet. Sci. Lett. 449, 118–126. https://doi.org/10.1016/j.epsl.2016.05.049.
Cawood, P.A., Zhao, G.C., Yao, J.L., Wang, W., Xu, Y.J., Wang, Y.J., 2018. Reconstructing South China in Phanerozoic and Precambrian supercontinents. Earth-Sci. Rev. 186, 173–194. https://doi.org/10.1016/j.earscirev.2017.06.001. Reconstruction of East Asian Continental Blocks in Pangea.
Cawood, P.A., Martin, E.L., Murphy, J.B., Pisarevsky, S.A., 2021. Gondwana's interlinked peripheral orogens. Earth Planet. Sci. Lett. 568, 117057. https://doi.org/10.1016/j.epsl.2021.117057.
Cawood, P.A., Chowdhury, P., Mulder, J.A., Hawkesworth, C.J., Capitanio, F.A., Gunawardana, P.M., Nebel, O., 2022. Secular evolution of continents and the earth system. Rev. Geophys. 60 (4). https://doi.org/10.1029/2022RG000789 e2022RG000789.
Chardon, D., Gapais, D., Cagnard, F., 2009. Flow of ultra-hot orogens: a view from the Precambrian, clues for the Phanerozoic. Tectonophysics 477 (3–4), 105–118. https://doi.org/10.1016/j.tecto.2009.03.008.
Chen, K., Rudnick, R.L., Wang, Z.C., Tang, M., Gaschnig, R.M., Zou, Z.Q., He, T., Hu, Z.C., Liu, Y.S., 2020. How mafic was the Archean upper continental crust? Insights from Cu and Ag in ancient glacial diamictites. Geochim. Cosmochim. Acta 278, 16–29. https://doi.org/10.1016/j.gca.2019.08.002.
DeCelles, P.G., Ducea, M.N., Kapp, P., Zandt, G., 2009. Cyclicity in Cordilleran orogenic systems. Nat. Geosci. 2, 251–257. https://doi.org/10.1038/ngeo469.
Dickinson, W.R., 2004. Evolution of the north American Cordillera. Annu. Rev. Earth Planet. Sci. 32, 13–45. https://doi.org/10.1146/annurev.earth.32.101802.120257.
Dong, Y.P., Liu, X.M., Santosh, M., Zhang, X.N., Chen, Q., Yang, C., Yang, Z., 2011. Neoproterozoic subduction tectonics of the northwestern Yangtze Block in South China: constrains from zircon U–Pb geochronology and geochemistry of mafic intrusions in the Hannan Massif. Precambrian Res. 189 (1–2), 66–90. https://doi.org/10.1016/j.precamres.2011.05.002.
Dong, Y.P., Liu, X.M., Santosh, M., Chen, Q., Zhang, X.N., Li, W., He, D.F., Zhang, G.W., 2012. Neoproterozoic accretionary tectonics along the northwestern margin of the Yangtze Block, China: constraints from zircon U–Pb geochronology and geochemistry. Precambrian Res. 196–197, 247–274. https://doi.org/10.1016/j.precamres.2011.12.007.
Dong, Y.P., Hui, B., Sun, S.S., He, D.F., Sun, J.P., Zhang, F.F., Cheng, C., Yang, Z., Shi, X. H., Zang, R.T., Long, X.P., Zhang, G.W., 2024. Neoproterozoic tectonic evolution and proto-basin of the Yangtze block, China. Earth-Sci. Rev. 249, 104669. https://doi.org/10.1016/j.earscirev.2023.104669.
Ducea, M.N., Saleeby, J.B., Bergantz, G., 2015. The architecture, chemistry, and evolution of continental magmatic arcs. Annu. Rev. Earth Planet. Sci. 43, 299–331. https://doi.org/10.1146/annurev-earth-060614-105049.
Farner, M.J., Lee, C.T.A., 2017. Effects of crustal thickness on magmatic differentiation in subduction zone volcanism: a global study. Earth Planet. Sci. Lett. 470, 96–107. https://doi.org/10.1016/j.epsl.2017.04.025.
Gao, S., Yang, J., Zhou, L., Li, M., Hu, Z.C., Guo, J.L., Yuan, H.L., Gong, H.J., Xiao, G.Q., Wei, J.Q., 2011. Age and growth of the Archean Kongling Terrain, South China, with Emphasis on 3.3 Ga Granitoid Gneisses. Am. J. Sci. 311 (2), 153–182. https://doi.org/10.2475/02.2011.03.
Gerya, T., 2014. Precambrian geodynamics: concepts and models. Gondwana Res. 25 (2), 442–463. https://doi.org/10.1016/j.gr.2012.11.008.
Griffin, W.L., Pearson, N.J., Belousova, E., Jackson, S.E., van Achterbergh, E., O'Reilly, S. Y., Shee, S.R., 2000. The Hf isotope composition of cratonic mantle: LAM-MC-ICPMS analysis of zircon megacrysts in kimberlites. Geochim. Cosmochim. Acta 64 (1), 133–147. https://doi.org/10.1016/S0016-7037(99)00343-9.
Griffin, W.L., Belousova, E.A., Shee, S.R., Pearson, N.J., O'Reilly, S.Y., 2004. Archean crustal evolution in the northern Yilgarn Craton: U–Pb and Hf-isotope evidence from detrital zircons. Precambrian Res. 131 (3–4), 231–282. https://doi.org/10.1016/j.precamres.2003.12.011.
Grimes, C.B., Wooden, J.L., Cheadle, M.J., John, B.E., 2015. "Fingerprinting" tectono-magmatic provenance using trace elements in igneous zircon. Contrib. Mineral. Petrol. 170, 46. https://doi.org/10.1007/s00410-015-1199-3.
Gu, Z., Wang, Z., 2014. The discovery of Neoproterozoic extensional structures and its significance for gas exploration in the Central Sichuan block, Sichuan basin, South China. Sci. China Earth Sci. 57, 2758–2768. https://doi.org/10.1007/s11430-014-4961-x.
Guo, Q.P., Chen, Y.L., Fan, W., Fu, Y.Z., Gu, M.J., Zhang, B.L., Zhai, G.X., 2024. Temperature and pressure Conditions Research of Metamorphism of the Pudeng Formation, Julin Group in the Xujie area of Mouding Country, Yunnan Province. Acta Geol. Sichuan 44, 579–587 (In Chinese with English abstract).
Hawkesworth, C.J., Cawood, P.A., Dhuime, B., 2016. Tectonics and crustal evolution. Geol. Soc. Am. Today 26 (9), 4–11.
He, Y., Wu, Y.B., Zhao, Y.J., Xiang, H., Hu, Z.C., Zhou, G.Y., 2023. Neoproterozoic amphibolite-facies metamorphism of the Douling complex in the northern Yangtze Craton and its tectonic implications: Constraints from petrology and zircon U-Pb-Hf-O isotopes. Precambrian Res. 390, 107039. https://doi.org/10.1016/j.precamres.2023.107039.
Huang, X.L., Xu, Y.G., Li, X.H., Li, W.X., Lan, J.B., Zhang, H.H., Liu, Y.L., Wang, Y.B., Li, H.Y., Luo, Z.Y., Yang, Q.J., 2008. Petrogenesis and tectonic implications of Neoproterozoic, highly fractionated A-type granites from Mianning, South China. Precambrian Res. 165, 190–204. https://doi.org/10.1016/j.precamres.2008.06.010.
Huang, H.Y., He, D.F., Li, D., Li, Y.Q., 2021a. Zircon U-Pb ages and Hf isotope analysis of Neoproterozoic Yaolinghe group sedimentary rocks in the Chengkou area, south Qinling: provenance and paleogeographic implications. Precambrian Res. 355, 106088. https://doi.org/10.1016/j.precamres.2020.106088.
Huang, Y., Wang, X.L., Li, J.Y., Wang, D., Jiang, C.H., Li, L.S., 2021b. Early Neoproterozoic tectonic evolution of northern Yangtze block: insights from sedimentary sequences from the Dahongshan area. Precambrian Res. 365, 106382. https://doi.org/10.1016/j.precamres.2021.106382.
Hynes, A., Rivers, T., 2010. Protracted continental collision — evidence from the Grenville Orogen. Can. J. Earth Sci. 47, 591–620. https://doi.org/10.1139/E10-003.
Johansson, Å., 2009. Baltica, Amazonia and the SAMBA connection—1000 million years of neighbourhood during the Proterozoic? Precambrian Res. 175 (1–4), 221–234. https://doi.org/10.1016/j.precamres.2009.09.011.
Kemp, A.I.S., Hawkesworth, C.J., Foster, G.L., Paterson, B.A., Woodhead, J.D., Hergt, J. M., Gray, C.M., Whitehouse, M.J., 2007. Magmatic and crustal differentiation history of granitic rocks from Hf-O Isotopes in Zircon. Science 315 (5814), 980–983.
Larsen, I.J., Montgomery, D.R., Greenberg, H.M., 2014. The contribution of mountains to global denudation. Geology 42 (6), 527–530. https://doi.org/10.1130/G35136.1.
Lee, C.T.A., Tang, M., 2020. How to make porphyry copper deposits. Earth Planet. Sci. Lett. 529, 115868. https://doi.org/10.1016/j.epsl.2019.115868.
Lee, C.T.A., Thurner, S., Paterson, S., Cao, W., 2015. The rise and fall of continental arcs: interplays between magmatism, uplift, weathering, and climate. Earth Planet. Sci. Lett. 425, 105–119. https://doi.org/10.1016/j.epsl.2015.05.045.
Li, X.H., Long, W.G., Li, Q.L., Liu, Y., Zheng, Y.F., Yang, Y.H., Chamberlain, K.R., Wan, D. F., Guo, C.H., Wang, X.C., Tao, H., 2010. Penglai zircon megacrysts: a potential new working reference material for microbeam determination of Hf–O isotopes and U–Pb Age. Geostand. Geoanal. Res. 34 (2), 117–134. https://doi.org/10.1111/j.1751-908X.2010.00036.x.
Li, J.Y., Wang, X.L., Gu, Z.D., 2018. Early Neoproterozoic arc magmatism of the Tongmuliang Group on the northwestern margin of the Yangtze Block: implications for Rodinia assembly. Precambrian Res. 309, 181–197. https://doi.org/10.1016/j.precamres.2017.04.040.
Li, K.Z., Deng, Q., Hou, M.C., Wang, J., Yakymchuk, C., Cui, X.Z., Ren, G.M., Wang, Z.J., 2020. Geochronology and sedimentology of the Huashan group in the northern Yangtze Block: implications for the initial breakup of the South China. Int. J. Earth Sci. 109, 2113–2131. https://doi.org/10.1007/s00531-020-01890-0.
Li, J.Y., Tang, M., Lee, C.T.A., Wang, X.L., Gu, Z.D., Xia, X.P., Wang, D., Du, D.H., Li, L.S., 2021a. Rapid endogenic rock recycling in magmatic arcs. Nat. Commun. 12, 3533. https://doi.org/10.1038/s41467-021-23797-3.
Li, Z.M.G., Chen, Y.C., Zhang, Q.W.L., Liu, J.H., Wu, C.M., 2021b. U-Pb dating of metamorphic monazite of the Neoproterozoic Kang-Dian Orogenic Belt, southwestern China. Precambrian Res. 361, 106262. https://doi.org/10.1016/j.precamres.2021.106262.
Li, Z.M.G., Chen, Y.C., Zhang, Q.W.L., Liu, J.H., Wu, C.M., 2022. P-T conditions and timing of metamorphism of the Yuanmou area, southern Neoproterozoic Kang-Dian Orogenic Belt, Southwest China. Precambrian Res. 374, 106642. https://doi.org/10.1016/j.precamres.2022.106642.
Li, J.Y., Wang, X.L., Cawood, P.A., Gu, Z.D., Guan, Y., 2024. Neoproterozoic low-T/P metamorphism in the Yangtze Block manifests a long-lived subduction girdle around Rodinia. Earth Planet. Sci. Lett. 634, 118678. https://doi.org/10.1016/j.epsl.2024.118678.
Liu, H., Zhao, J.H., Cawood, P.A., Wang, W., 2018. South China in Rodinia: constrains from the neoproterozoic suixian volcano-sedimentary group of the South Qinling Belt. Precambrian Res. 314, 170–193. https://doi.org/10.1016/j.precamres.2018.05.018.
Mitchell, R.N., Zhang, N., Salminen, J., Liu, Y.B., Spencer, C.J., Steinberger, B., Murphy, J.B., Li, Z.X., 2021. The supercontinent cycle. Nat. Rev. Earth Environ. 2, 358–374. https://doi.org/10.1038/s43017-021-00160-0.
Murphy, J.B., Nance, R.D., 1991. Supercontinent model for the contrasting character of late Proterozoic orogenic belts. Geology 19 (5), 469–472. https://doi.org/10.1130/0091-7613(1991)019<0469:SMFTCC>2.3.CO;2.
Palin, R.M., Santosh, M., Cao, W.T., Li, S.S., Hernández-Uribe, D., Parsons, A., 2020. Secular change and the onset of plate tectonics on Earth. Earth Sci. Rev. 207, 103172. https://doi.org/10.1016/j.earscirev.2020.103172.
Perchuk, A.L., Safonov, O.G., Smit, C.A., van Reenen, D.D., Zakharov, V.S., Gerya, T.V., 2018. Precambrian ultra-hot orogenic factory: making and reworking of continental crust. Tectonophysics 746, 572–586. https://doi.org/10.1016/j.tecto.2016.11.041.
Profeta, L., Ducea, M.N., Chapman, J.B., Paterson, S.R., Gonzales, S.M.H., Kirsch, M., Petrescu, L., DeCelles, P.G., 2015. Quantifying crustal thickness over time in magmatic arcs. Sci. Rep. 5, 17786. https://doi.org/10.1038/srep17786.
Roberts, N.M.W., Salminen, J., Johansson, Å., Mitchell, R.N., Palin, R.M., Condie, K.C., Spencer, C.J., 2022. On the enigmatic mid-Proterozoic: Single-lid versus plate tectonics. Earth Planet. Sci. Lett. 594, 117749. https://doi.org/10.1016/j.epsl.2022.117749.

Roberts, N.M.W., Yakymchuk, C., Spencer, C.J., Keller, C.B., Tapster, S.R., 2024. Revisiting the discrimination and distribution of S-type granites from zircon trace element composition. Earth Planet. Sci. Lett. 633, 118638. https://doi.org/10.1016/j.epsl.2024.118638.

Shu, L.S., 2012. An analysis of principal features of tectonic evolution in South China Block. Geol. Bull. China 31 (7), 1035–1053 (In Chinese with English abstract).

Shu, L.S., Yao, J.L., Wang, B., Faure, M., Charvet, J., Chen, Y., 2021. Neoproterozoic plate tectonic process and Phanerozoic geodynamic evolution of the South China Block. Earth Sci. Rev. 216, 103596. https://doi.org/10.1016/j.earscirev.2021.103596.

Spencer, C.J., Cawood, P.A., Hawkesworth, C.J., Prave, A.R., Roberts, N.M.W., Horstwood, M.S.A., Whitehouse, M.J., 2015. Generation and preservation of continental crust in the Grenville Orogeny. Geosci. Front. 6 (3), 357–372. https://doi.org/10.1016/j.gsf.2014.12.001.

Spencer, C.J., Kirkland, C.L., Taylor, R.J.M., 2016. Strategies towards statistically robust interpretations of in situ U–Pb zircon geochronology. Geosci. Front. 7 (4), 581–589. https://doi.org/10.1016/j.gsf.2015.11.006.

Spencer, C.J., Murphy, J.B., Hoiland, C.W., Johnston, S.T., Mitchell, R.N., Collins, W.J., 2019. Evidence for whole mantle convection driving cordilleran tectonics. Geophys. Res. Lett. 46 (8), 4239–4248. https://doi.org/10.1029/2019GL082313.

Spencer, C.J., Mitchell, R.N., Brown, M., 2021. Enigmatic mid-proterozoic orogens: hot, thin, and Low. Geophys. Res. Lett. 48 (16). https://doi.org/10.1029/2021GL093312 e2021GL093312.

Stern, R.J., 2005. Evidence from ophiolites, blueschists, and ultrahigh-pressure metamorphic terranes that the modern episode of subduction tectonics began in Neoproterozoic time. Geology 33 (7), 557–560. https://doi.org/10.1130/G21365.1.

Sun, W.H., Zhou, M.F., Gao, J.F., Yang, Y.H., Zhao, X.F., Zhao, J.H., 2009. Detrital zircon U–Pb geochronological and Lu-Hf isotopic constraints on the Precambrian magmatic and crustal evolution of the western Yangtze Block, SW China. Precambrian Res. 172 (1–2), 99–126. https://doi.org/10.1016/j.precamres.2009.03.010.

Tang, M., Erdman, M., Eldridge, G., Lee, C.T.A., 2018. The redox "filter" beneath magmatic orogens and the formation of continental crust. Sci. Adv. 4 (5), eaar4444. https://doi.org/10.1126/sciadv.aar4444.

Tang, M., Ji, W.Q., Chu, X., Wu, A., Chen, C., 2021. Reconstructing crustal thickness evolution from europium anomalies in detrital zircons. Geology 49 (1), 76–80. https://doi.org/10.1130/G47745.1.

Tang, M., Guo, Z.Y., Cao, W.R., Chu, X., 2024. Revisiting zircon Eu anomaly as a proxy for crustal thickness: a case study of the Sierra Nevada Batholith. Earth Planet. Sci. Lett. 643, 118897. https://doi.org/10.1016/j.epsl.2024.118897.

Valley, J.W., Kinny, P.D., Schulze, D.J., Spicuzza, M.J., 1998. Zircon megacrysts from kimberlite: oxygen isotope variability among mantle melts. Contrib. Mineral. Petrol. 133, 1–11. https://doi.org/10.1007/s004100050432.

Valley, J.W., Bindeman, I.N., Peck, W.H., 2003. Empirical calibration of oxygen isotope fractionation in zircon. Geochim. Cosmochim. Acta 67 (17), 3257–3266. https://doi.org/10.1016/S0016-7037(03)00090-5.

Wang, X.L., Zhou, J.C., Griffin, W.L., Wang, R.C., Qiu, J.S., O'Reilly, S.Y., Xu, X., Liu, X.M., Zhang, G.L., 2007. Detrital zircon geochronology of Precambrian basement sequences in the Jiangnan orogen: dating the assembly of the Yangtze and Cathaysia Blocks. Precambrian Res. 159 (1–2), 117–131. https://doi.org/10.1016/j.precamres.2007.06.005.

Wang, X.C., Li, Z.X., Li, X.H., Li, Q.L., Tang, G.Q., Zhang, Q.R., Liu, Y., 2011. Nonglacial origin for low-δ18O Neoproterozoic magmas in the South China Block: evidence from new in-situ oxygen isotope analyses using SIMS. Geology 39 (8), 735–738. https://doi.org/10.1130/G31991.1.

Wang, X.C., Li, X.H., Li, Z.X., Li, Q.L., Tang, G.Q., Gao, Y.Y., Zhang, Q.R., Liu, Y., 2012. Episodic Precambrian crust growth: evidence from U–Pb ages and Hf–O isotopes of zircon in the Nanhua Basin, central South China. Precambrian Res. 222–223, 386–403. https://doi.org/10.1016/j.precamres.2011.06.001.

Wang, L.J., Griffin, W.L., Yu, J.H., O'Reilly, S.Y., 2013. U-Pb and Lu-Hf isotopes in detrital zircon from Neoproterozoic sedimentary rocks in the northern Yangtze Block: implications for Precambrian crustal evolution. Gondwana Res. 23 (4), 1261–1272. https://doi.org/10.1016/j.gr.2012.04.013.

Wang, X.L., Zhou, J.C., Griffin, W.L., Zhao, G.C., Yu, J.H., Qiu, J.S., Zhang, Y.J., Xing, G.F., 2014. Geochemical zonation across a Neoproterozoic orogenic belt: Isotopic evidence from granitoids and metasedimentary rocks of the Jiangnan orogen, China. Precambrian Res. 242, 154–171. https://doi.org/10.1016/j.precamres.2013.12.023.

Wang, W., Cawood, P.A., Zhou, M.F., Pandit, M.K., Xia, X.P., Zhao, J.H., 2017a. Low-δ^{18}O Rhyolites from the Malani Igneous Suite: a positive Test for South China and NW India Linkage in Rodinia. Geophys. Res. Lett. 44. https://doi.org/10.1002/2017GL074717.

Wang, X.L., Zhou, J.C., Chen, X., Zhang, F.F., Sun, Z.M., 2017b. Formation and evolution of the Jiangnan Orogen. Bull. Mineral. Petrol. Geochem. 36 (5), 714–735 (In Chinese with English abstract). https://doi.org/10.3969/j.issn.1007-2802.2017.05.003.

Wang, H.Z., Oscar, L., Zhang, H.F., Zhang, H., Chen, X., Zhai, M.G., 2020. Recognition and significance of c. 800 Ma upper amphibolite to granulite facies metamorphism in metasedimentary rocks from the NW margin of the Yangtze block. J. Geol. Soc. Lond. 177, 424–441. https://doi.org/10.1144/jgs2019-035.

Wu, P., Zhang, S.B., Zheng, Y.F., Fu, B., Liang, T., 2019. Amalgamation of South China into Rodinia during the Grenvillian accretionary orogeny: geochemical evidence from early Neoproterozoic igneous rocks in the northern margin of the South China Block. Precambrian Res. 321, 221–243. https://doi.org/10.1016/j.precamres.2018.12.015.

Wu, G.H., Chu, X., Tang, M., Li, W.Y., Chen, F.K., 2023a. Distinct tectono-magmatism on the margins of Rodinia and Gondwana. Earth Planet. Sci. Lett. 609, 118099. https://doi.org/10.1016/j.epsl.2023.118099.

Wu, P., Zhang, S.B., Li, Z.X., Wu, Y.B., Zheng, Y.F., 2023b. Secular change in the nature of mantle and tectonic evolution of northwestern margin of the Yangtze block during Neoproterozoic: constraints from the mafic intrusions and associated granitoids of the Hannan and Xiaomoling complexes. Precambrian Res. 393, 107094. https://doi.org/10.1016/j.precamres.2023.107094.

Wu, P., Wu, Y.B., Zhang, S.B., Zheng, Y.F., Li, L., Gao, Y., Song, H., Xu, Z.Q., Shi, Z.M., 2024. Revisiting Neoproterozoic tectono-magmatic evolution of the northern margin of the Yangtze Block, South China. Earth-Sci. Rev. 255, 104825. https://doi.org/10.1016/j.earscirev.2024.104825.

Xiong, D.Y., Wang, X.L., Xing, G.F., 2023a. A supercontinental cycles perspective for the formation of Precambrian pegmatitic lithium deposits. East China Geol. 44 (1), 1–12 (In Chinese with English abstract).

Xiong, F., Liu, Q., Hou, M., Yan, S., 2023b. Petrogenesis of Neoproterozoic mafic dykes in western Yangtze Block, South China: implications for the assembly and break-up of Rodinia. Int. Geol. Rev. 65, 2191–2211. https://doi.org/10.1080/00206814.2022.2129474.

Yang, Y.N., Wang, X.C., Li, Q.L., Li, X.H., 2016. Integrated in situ U–Pb age and Hf–O analyses of zircon from Suixian Group in northern Yangtze: new insights into the Neoproterozoic low-δ18O magmas in the South China Block. Precambrian Res. 273, 151–164. https://doi.org/10.1016/j.precamres.2015.12.008.

Yang, Z.N., Yang, K.G., Polat, A., Xu, Y., 2018. Early crustal evolution of the eastern Yangtze Block: evidence from detrital zircon U-Pb ages and Hf isotopic composition of the Neoproterozoic Huashan Group in the Dahongshan area. Precambrian Res. 309, 248–270. https://doi.org/10.1016/j.precamres.2017.05.011.

Yang, Z., Cawood, P.A., Zi, J.W., Gou, L.L., Liu, G.C., Liu, R., Xu, X.F., 2024. Mid-Neoproterozoic (ca. 845 Ma) metamorphism of the southwestern Yangtze Block and its tectonic implications. Precambrian Res. 400, 107267. https://doi.org/10.1016/j.precamres.2023.107267.

Yao, J.L., Cawood, P.A., Shu, L.S., Zhao, G.C., 2019. Jiangnan Orogen, South China: a ~970–820 Ma Rodinia margin accretionary belt. Earth Sci. Rev. 196, 102872. https://doi.org/10.1016/j.earscirev.2019.05.016.

Zhang, C.L., Li, Z.X., Li, X.H., Ye, H.M., 2009. Neoproterozoic mafic dyke swarms at the northern margin of the Tarim Block, NW China: age, geochemistry, petrogenesis and tectonic implications. J. Asian Earth Sci. 35 (2), 167–179. https://doi.org/10.1016/j.jseaes.2009.02.003.

Zhao, G.C., Cawood, P.A., 2012. Precambrian geology of China. Precambrian Res. 222–223, 13–54. https://doi.org/10.1016/j.precamres.2012.09.017.

Zhao, J.H., Zhou, M.F., 2007. Geochemistry of Neoproterozoic mafic intrusions in the Panzhihua district (Sichuan Province, SW China): implications for subduction-related metasomatism in the upper mantle. Precambrian Res. 152 (1–2), 27–47. https://doi.org/10.1016/j.precamres.2006.09.002.

Zhao, J.H., Zhou, M.F., 2009. Secular evolution of the Neoproterozoic lithospheric mantle underneath the northern margin of the Yangtze Block, South China. Lithos 107 (3–4), 152–168. https://doi.org/10.1016/j.lithos.2008.09.017.

Zhao, X.F., Zhou, M.F., Li, J.W., Wu, F.Y., 2008. Association of Neoproterozoic A- and I-type granites in South China: implications for generation of A-type granites in a subduction-related environment. Chem. Geol. 257, 1–15. https://doi.org/10.1016/j.chemgeo.2008.07.018.

Zhao, J.H., Zhou, M.F., Wu, Y.B., Zheng, J.P., Wang, W., 2019. Coupled evolution of Neoproterozoic arc mafic magmatism and mantle wedge in the western margin of the South China Craton. Contrib. Mineral. Petrol. 174, 36. https://doi.org/10.1007/s00410-019-1573-7.

Zhao, J.H., Nebel, O., Johnson, T.E., 2021. Formation and evolution of a neoproterozoic continental magmatic arc. J. Petrol. 62 (8), egab029. https://doi.org/10.1093/petrology/egab029.

Zhao, L.M., Li, Y.L., Rong, C., Li, F.L., Xiang, H., Zheng, J.P., Brouwer, F.M., 2022. Geochemical and zircon U-Pb-Hf isotopic study of volcanic rocks from the Yaolinghe Group, South Qinling orogenic belt, China: constraints on the assembly and breakup of Rodinia. Precambrian Res. 371, 106603. https://doi.org/10.1016/j.precamres.2022.106603.

Zhou, M.F., Kennedy, A.K., Sun, M., Malpas, J., Lesher, C.M., 2002. Neoproterozoic Arc-Related Mafic Intrusions along the Northern margin of South China: implications for the accretion of Rodinia. J. Geol. 110, 611–618. https://doi.org/10.1086/341762.

Zhu, X.Y., Chen, F.K., Yang, L., Wang, W., Hieu, P.T., Miao, L.C., Zhang, F.Q., 2009. Zircon Hf isotopic composition and source characteristics of the Wudang Group in the Qinling orogenic belt, western Henan province. Acta Petrol. Sin. 25 (11), 3017–3028 (In Chinese with English abstract).

Zhu, Y., Lai, S., Qin, J., Zhu, R., Zhang, F., Zhang, Z., Gan, B., 2019. Petrogenesis and geodynamic implications of Neoproterozoic gabbro-diorites, adakitic granites, and a-type granites in the southwestern margin of the Yangtze block, South China. J. Asian Earth Sci. 183, 103977. https://doi.org/10.1016/j.jseaes.2019.103977.